Investigation of the flow field downstream of an artificial heart valve by means of PIV and PTV

A. Balducci, M. Grigioni, G. Querzoli, G.P. Romano, C. Daniele, G. D'Avenio, V. Barbaro

Abstract Measurements of the velocity field downstream of an artificial heart valve are performed by using particle image velocimetry (PIV) and particle tracking velocimetry (PTV). The investigated field corresponds to the region immediately downstream of the valve outlet i.e. the initial ascending part of the aorta. The aim of the paper is to investigate the evolution of the flow field in time in such inhomogeneous, anisotropic, and unsteady conditions. To do this, a high-speed video camera is used to acquire images of the seeding particles illuminated by a continuous infrared laser. high seeding density conditions are investigated using PIV to perform phase-sampled Eulerian averages, whereas low seeding conditions are used to determine particle trajectories and Lagrangian statistics using PTV. Both are needed for the complete description of the magnitude and duration of the stress on blood cells. The following features are described:

– The very high inhomogeneity and unsteadiness of the phenomenon
– The presence of large scale vortices within the field especially in the sinuses of Valsalva and in the wake of the valve leaflets
– The strong stress and strain rates at the jet–wake interface downstream of the leaflets and close to large-scale vortices
– The non-negligible time spent by fluid particles in some of the high stress and strain regions

A. Balducci, G.P. Romano (✉)
Department of Mechanics and Aerodynamics,
University "La Sapienza", Roma, Italy
E-mail: romano@dma.ing.uniroma1.it

M. Grigioni, C. Daniele, G. D'Avenio, V. Barbaro
Laboratory of Biomedical Engineering,
Istituto Superiore di Sanità, Roma, Italy

G. Querzoli
Dipartimento di Ingegneria del Territorio,
University of Cagliari, Italy

1
Motivation and objectives

Great interest has recently arisen for the investigation of biological flows using new analysis techniques. This interest involves not only special applications related to crucial diseases for the life of many people, but even on challenging problems for advanced numerical and experimental methods used in fluid mechanics. In particular, it has been reported that the blood shear stress field is closely involved in specific diseases; low shear regions induce settling of the heaviest blood components and thromboses, while high shear regions stretch and damage blood cells (Fung 1985; Ku 1997; Grigioni et al. 1999).

Here, we focus on the flow field downstream of an artificial heart valve. Such a flow field has a complex geometry and is characterised by very high velocity gradients both in space and time. To quantify these aspects, it is important to stress that the characteristic features of this problem are the order of magnitude of the inertial terms in the Navier-Stokes equations, which are as large as 10^3 m s^{-2} (the maximum Reynolds number, Re, based on the maximum velocity and valve diameter, is between 5,000 and 10,000), and the Womersley number (equal to $\sqrt{Re\ St}$, where St is the Strouhal number), which is larger than 10.

In particular, the design of modern artificial heart valves, while involving several problems concerning the materials, the shape, and the geometry of the valve, should also focus on avoiding undesired strong fluid-mechanical effects, that is:

– Minimise the damaging effect of the flow field (and in particular of the stress field) on blood cells (hemolysis and thrombus formation) (Grigioni et al. 1999; Lu et al. 2001)
– Allow the flow field downstream of the artificial valve to reproduce the physiological field
– Reduce as much as possible the backflow which affects the valve closing and the leakage phase, at the same time maintaining an adequate washout of the valve components

These fundamental tasks cannot be solved without a detailed investigation of the fluid mechanics field. However, the unsteady, inhomogeneous, and anisotropic nature of such a flow field should be considered. It is also very important to consider that the required information on the flow field (mean velocity, *rms*, and stress values) must be provided simultaneously in a Eulerian framework (to identify the regions where characteristic phenomena are

observed) and in a Lagrangian framework (to follow blood elements along their trajectories and to determine cumulative effects (Bludszuweit 1995; Zimmer et al. 2000; Grigioni et al. 2001).

Although advanced numerical methods operate with similar complex geometries and can work with both Eulerian and Lagrangian approaches, they do not always achieve the appropriate high resolutions (especially in time). This is why an experimental approach is still needed. Moreover, in the ascending aorta, during the systole, the peak Reynolds number is up to 9,000, which leads to a fully developed turbulent flow (Ku 1997). In such a complex and confined flow field, optical methods for velocity measurements are required, although their use in these conditions is not straightforward. Among them, the use of image analysis velocimetry techniques [including particle image velocimetry (PIV) and particle tracking velocimetry (PTV)] now attains the desired high spatial and temporal resolutions; by changing the seeding density conditions, it is also possible to derive information in a Eulerian (PIV and PTV) or a Lagrangian (PTV) framework.

In this paper, the velocity field at the outlet of a flat bi-leaflet artificial heart valve is investigated using PIV and PTV. The investigated field corresponds to the region immediately downstream of the artificial valve outlet, i.e. the aortic root. The aim of the paper is to investigate the evolution of the flow field in time using a high-speed video-camera; the PIV technique is used in high seeding density conditions to perform phase-sampled Eulerian averages, whereas low seeding is used to determine particle trajectories and Lagrangian statistics using PTV.

2
Experimental set-up

The present experimental study is performed over a 1:1 model of the aortic root downstream of an artificial bi-leaflet heart valve. The determination of the correct artificial valve to be used in a given condition has involved several scientists in the last years; the bi-leaflet valves gained success in the market as the one which better reproduces the most important physiological features. In this work, the attention is not focussed on the determination of an optimal artificial valve, but rather on how to derive information useful for biomedical purposes from a multi-point measurement technique.

Concerning the set-up of the experimental apparatus (shown in Fig. 1), which simulates the initial part of the aorta downstream of the valve, it is important to point out that several phenomena should be taken into account for a proper simulation. Particular care is given to the following items (Barbaro et al. 1998):

– The working fluid is selected in order to reproduce the kinematics and dynamics of the blood but still preserve the fluid transparency to allow optical access. A solution of de-ionised water and glycerol with a small fraction of sodium chloride for EM flow-meter function is used.
– The geometry of the aorta (made from blown glass) corresponds as much as possible to the physiological case with the correct scaling (as reported in Fig. 1b); at the outlet of the valve, the three sinuses of Valsalva are placed at equispaced radial positions (120°); however, for prosthetic valves, in comparison to the physiological conditions, the sinuses are not filled by muscular tissues, so that their role in the fluid dynamics should be different (Reul et al. 1993).
– The elastic properties of the aorta walls are considered by inserting a windkessel model for compensation into the hydraulic circuit which reproduces the systemic circulation; the pressure in the system is controlled through pressure taps positioned along the circuit (shown in Fig. 1a).
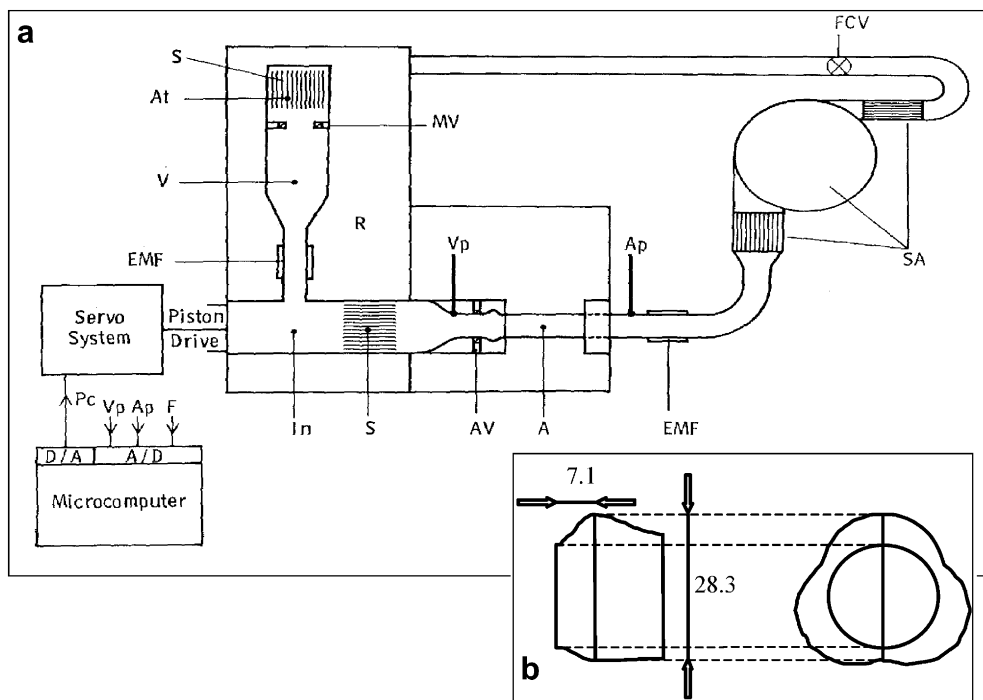
Fig. 1a, b. The schematic diagram of the experimental set-up from Barbaro et al. (1998). a *R*—Reservoir, *S*—Honeycomb, *At*—Atrium, *Mv*—Mitral valve, *V*—Ventricle, *EMF*—Electromagnetic flowmeter, *In*—Aortic inflow section, *Av*—Aortic valve, *Vp*—Ventricular pressure transducer, *AP*—Aortic pressure transducer, *A*—Model of the aortic root, *SA*—Model of the systemic circulation, *FCV*—Flow control valve, *D/A*—Digital-analogical converter, *Pc*—Position control, *Vp*—Ventricular pressure signal, *Ap*—Aortic pressure signal, *F*—Flow signal. b A detail of the ascending part of the aorta with the measurement section (measurements in mm)

– The driving system reproducing the periodic heart flow is provided by a mechanical system consisting of a motor, a transmission screw, and a piston; the wave forms used to control the system are generated by a computer with a position transducer as feedback control.

Due to the previously described geometry and depending on the prosthetic valve standard, the flow field is really three-dimensional and measurements on a single plane can highlight only a part of the phenomenon; nonetheless, it is particularly important to investigate the flow field in the region of the sinus of Valsalva on a plane orthogonal to the valve plane, where the highest stress is expected (on account of the high velocity gradients due to the three jet pattern imposed by the presence of two leaflets) (Fontaine et al. 1996). Nonetheless, it is clear that a full three-dimensional investigation of the flow field would be required; both PIV (stereo-PIV) and PTV (3D-PTV) will allow such a further investigation.

The behaviour in time of the ventricular and aortic pressure for the typical measurement conditions used in this work (mean flow rate equal to 1 l min^{-1}) are given in Fig. 2. As reported in the figure, the field is highly unsteady (especially the ventricular pressure) and the period of the heart cycle is about 0.8 s (the cycle starts when the ventricular pressure starts to rise); the points A and B correspond to intersections between the two pressure curves. They trigger the possibility for the valve to open (A) and to close (B) at given instants of the heart cycle. The mean aortic pressure is about 100 mmHg. In the same figure, the instantaneous flow rate is also given; it allows exact determination of the opening and closing of the valve. The opening of the valve starts at about 30 ms from the beginning of the cycle, while the maximum instantaneous flow rate is obtained at the systolic peak, i.e. at about 70 ms and the complete closing of the valve takes place at about 330 ms. In such a condition (as almost always in the cycle except for the systolic peak), there is a backflow towards the valve, which is typical of mechanical (prosthetic) heart valves. It should be noticed that there is not any apparent change in the pressure traces when the flow rate becomes negative; a possible explanation (which is also supported by the observation of the leaflet during the closing phase) is related to a delayed and protracted leaflet closure which could depend on the valve design. However, since the present measurements are performed at a mean flow rate equal to 1 l min^{-1}, i.e. quite far from physiological conditions, any speculation about the valve design derived from measurements in this regime should be avoided. The motivation for such a flow rate is connected to the limited frame rate of the image acquisition system (video-camera) which must be able to follow the instantaneous behaviour of the flow field (i.e. the evolution in time). The relatively low flow rate can also explain why the pressure difference before and after the systole is quite small (in the order of 10 mmHg). The velocity which is used as reference in the following is obtained from the maximum flow rate and is equal to about 0.626 m/s; using the valve nominal diameter as reference length (D=19 mm), thus the resulting Reynolds number is about 3,200.
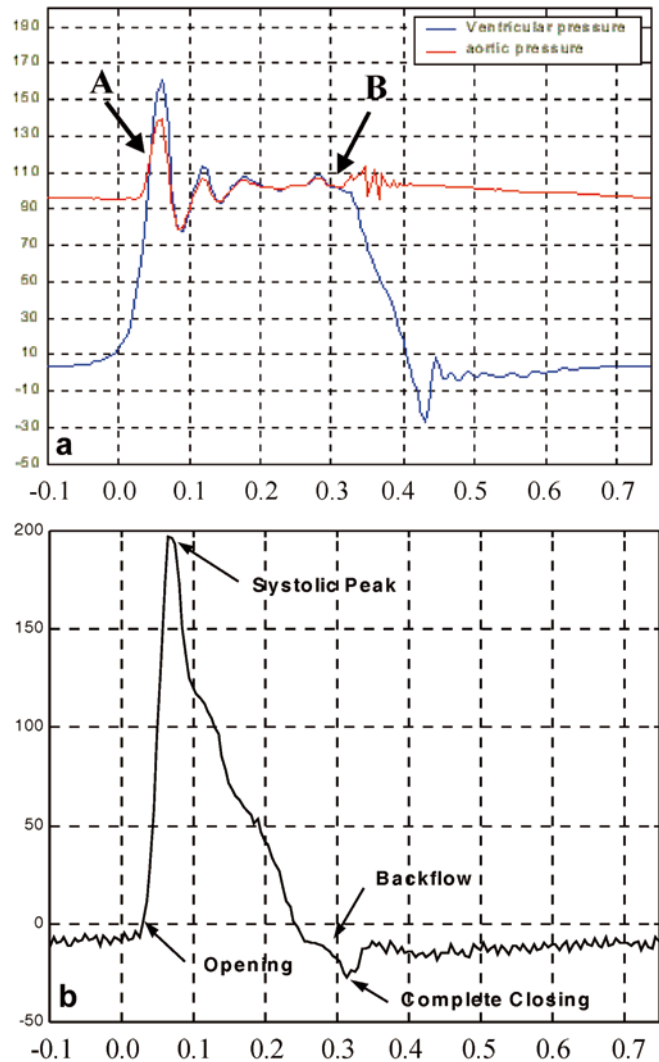

Fig. 2. Time variation (in s) of the ventricular and aortic pressure (in mmHg) (**a**) and of the instantaneous flow rate (in ml/s) (**b**) in a cardiac cycle using the apparatus of Fig. 1

The measurements region (about 3 cm × 2 cm, at the middle plane of the aortic arch) is illuminated by a light sheet from an infrared laser (power=12 W, wavelength=800 nm); the light scattered by strongly basic anion exchanging particles (mean size=10 μm) is acquired by a high-speed video-camera [frame rate=1 kHz, resolution (at this frame rate)=320 pixel×156 pixel] and transferred to a PC for further analysis. An example of the acquired images is given in Fig. 3a; the contours clearly show the boundaries of the measurement region with the artificial valve at the top and one sinus of Valsalva intersected by the measurement plane at the right side of the figure, the other two sinuses being symmetrically disposed at opposite sides of the measurement plane. The data are acquired at a discharge condition equal to about 1 l min^{-1}, at a mean aortic pressure equal to 100 mmHg; in terms of frame number, the periodicity of the phenomenon (0.8 s) is about 800 frames. About 60,000 images have been acquired, which correspond to about 90 periods; each image sequence is triggered by the driving system to perform phase sampling.
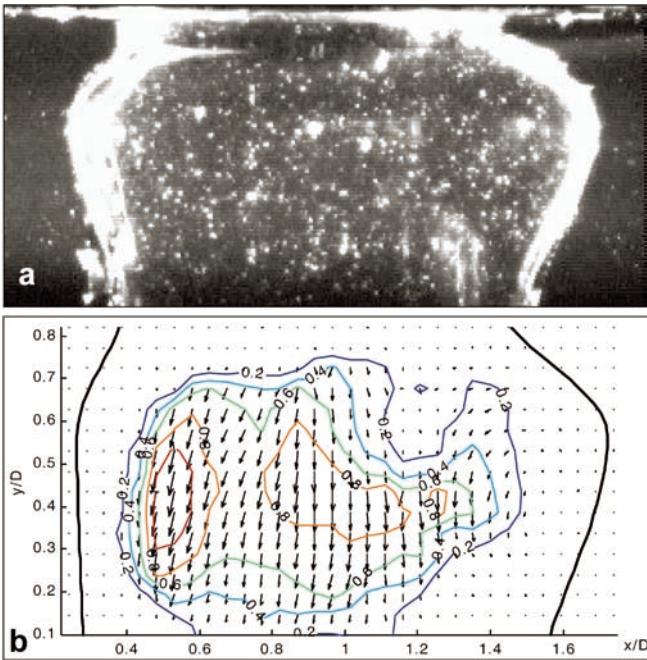
Fig. 3. Example of image acquisition (**a**) and image analysis using PIV (**b**) (the sinus of Valsalva is on the right) 90 ms after the beginning of the heart cycle. Frame rate equal to 1 kHz

Images are acquired within the limits of low and moderate particle concentrations which are considered optimal for image analysis using PTV and PIV, respectively. The former is performed using a frame by frame tracking procedure which allows one to derive particle trajectories and to compute Lagrangian statistics (Cenedese and Querzoli 2000). On the present flow field, it allows one to validate about 50 tracer images per frame and to follow them for several consecutive frames (from 10 up to about 50 depending on the phase of the flow). As typical for PTV, data are obtained at random positions in space and interpolation algorithms are required to derive results on a regular grid and to compute Eulerian statistics.

For PIV, the cross-correlation function of the intensity levels between consecutive frames is computed; the velocity on a plane is derived by analysing the peaks in the correlation plane (Adrian 1991). The use of a high-speed video-camera also enables one to follow the time evolution of the phenomenon with a quite high temporal resolution ($\Delta t=0.001$ s, $\Delta tU_{max}/D\approx0.05$). The PIV algorithm is a standard one which employs advanced improvements for image analysis by cross-correlation functions as the window offset and the sub-pixel Gaussian interpolation (AEA Visiflow); data have been validated also by using an advanced code developed recently (Di Florio et al. 2002). The image analysis was performed by using 32 pixel×32 pixel windows with 75% overlapping. Considering the camera resolution and the acquired region size, the minimum separation between velocity vectors measured by PIV is slightly less than 1 mm, i.e. the spatial resolution is quite high (contour maps are obtained by second-order polynomial interpolation of these velocity data). In Fig. 3b, an example of PIV analysis as obtained slightly before the systolic peak (90 ms

after the beginning of the heart cycle) is given; the axes x and y (non-dimensional by the valve diameter) are oriented respectively as parallel (transverse direction) and orthogonal (axial direction) to the plane of the valve and the corresponding velocity components are denoted as u and v. On the left side of Fig. 3b, the flow is mostly directed axially (initial section of the aorta), while on the right side there is a large recirculating region.

For both PTV and PIV data, due to the periodic nature of the flow field, images have to be analysed using phase averaging techniques; this means that averages are computed by considering velocity samples at the same phase for every cycle (the possibility of performing a time average has also been considered, but it has been excluded due to the observed strong unsteadiness of the phenomenon, especially during the systole). As described before, about 90 heart cycles are used so that each mean velocity value is obtained as the phase average of 90 independent samples (and similarly for the second-order moments, i.e. the *rms* velocities and the Reynolds stress, with a relative error which is evaluated to be in the order of 10%). The overall number of phase averaged velocity data in the heart cycle is equal to the heart cycle duration (0.8 s) times the frame rate (1,000 Hz), which is equal to about 800. The procedure described above allows evaluation of the evolution of the flow field in space (within each phase averaged field) and in time (between different phase averaged fields) as requested for the considered flow field.

3
Preliminary flow visualizations
Preliminary flow visualizations are performed using multi-exposure and long exposure image acquisition procedures; the frame rate and the shutter opening time (exposure time) are selected equal to 250 Hz (instead of 1 kHz used for PIV and PTV) and 1/250 s, respectively, so that the tracer particles appear as streaks on the images. In Fig. 4a, a multi-exposure image is given (three consecutive frames are overlapped in red, green, and blue, respectively); it corresponds to about 80 ms from the beginning of the heart cycle, i.e. immediately after the systolic peak. It is interesting to observe the formation of wake vortices downstream of the left leaflet (indicated by the left upper arrow) with growing size. They correspond to the wake of the leaflet within the accelerating flow field.

Due to the non-axisymmetric configuration, the previous features are different from those observed on the right-hand side of the field, within the sinus of Valsalva, where a recirculation region is forming. This is shown in greater detail in Fig. 4b and c (using long time exposure). Before the complete aperture of the valve (Fig. 4b), the flow still follows the sinus geometry without any major separation; after the aperture of the right leaflet (Fig. 4c) there is a vortex as large as the sinus, which moves within the sinus. From the length of the particle traces, the velocity within the field can be estimated to be larger than 1 m s^{-1}, i.e. substantially higher than the reference velocity derived from flow rate measurements. The behaviours noticed in these visualisations must be confirmed by quantitative measurements.
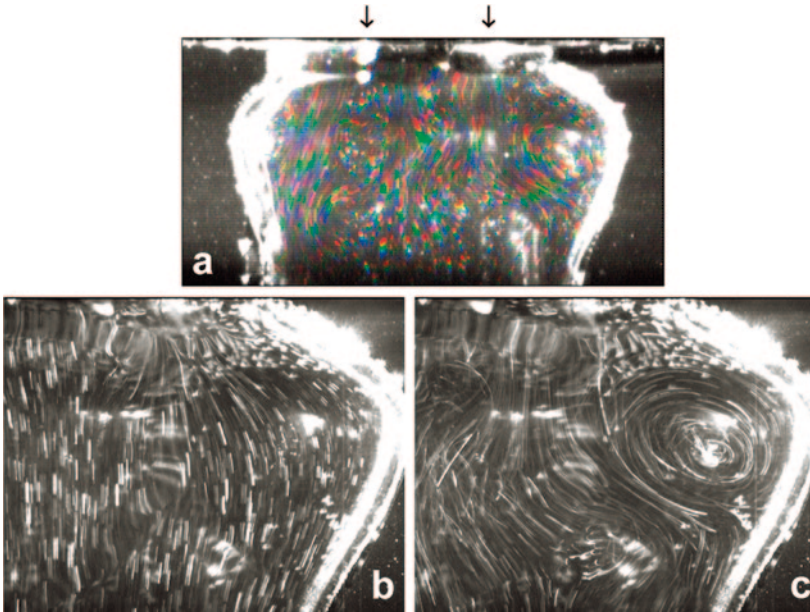
Fig. 4. Flow visualisations using multiple frame overlapping (3 frames) at the systolic peak (**a**) and long exposure time acquisitions (4 times the minimum time interval between frames, i.e. 1 ms) in the sinus of Valsalva (**b, c**). The *vertical arrows* indicate the position of the two leaflets when opened; images **b** and **c** correspond to 50 ms and 80 ms after the beginning of the cycle. Frame rate equal to 250 Hz

4
Results of PIV measurements

A sequence of eight phase-averaged vector fields derived from PIV measurements is given in Fig. 5;. In the figure, the time interval occurred after the beginning of the heart cycle; the position of the leaflets and the maximum positive or negative axial velocity are also shown for each field.

For a proper vortex identification, vorticity plots should not be used due to the fact that sometimes they hide vortical structures in shear flows. Jeong and Hussain (1995) proposed a vortex detection criterion based on the eigenvalues of the velocity gradient tensor which overcomes this problem.

In a two-dimensional flow, it is sufficient to verify that the following invariant quantity

$$\Delta = \left(\frac{\partial u}{\partial x} + \frac{\partial v}{\partial y}\right)^2 - 4\left(\frac{\partial u}{\partial x}\frac{\partial v}{\partial y} - \frac{\partial u}{\partial y}\frac{\partial v}{\partial x}\right)$$

is negative. The above criterion can be successfully extended to the two-dimensional analysis of three-dimensional flows (such as the one in this experiment) since they permit the identification of the vortices with the axis orthogonal to the investigated plane. Colour maps of the invariant Δ are overlapped onto the vector fields given in Fig. 5; they allow a clear identification of the vortical structures.

During the systole (which starts at $t=35$ ms), in about 40 ms the velocity abruptly rises from almost zero to 0.6 m/s. In this phase, the velocity vectors are directed almost axially all over the field except for small wakes downstream of the leaflet ($t=50–60$ ms). At the systolic peak ($t=65–70$ ms), two main vortical structures are observed in the wake of the leaflets (the one corresponding to the left leaflet being much more intense). Within the Valsalva sinus at least other two vortices are formed and they seem to interact during part of the cycle ($t=75–280$ ms). The size of the vortices is a remarkable fraction of the reference length (about 0.2–0.3 D), while their

trajectories (not shown) reveal that during the heart cycle they move downstream following the wall geometry of the sinus. During the reduced ejection ($t=120–280$ ms), the flow decelerates more slowly to an almost zero mean axial velocity (in about 200 ms); in this phase, the two vortical structures already observed within the sinus of Valsalva continue to interact with some change in the intensity (which represents the invariant quantity Δ). After this phase, the velocity almost vanishes even if a small back-flow (already noticed in the instantaneous flow rate given in Fig. 2b) is observed. These observations confirm the fact that the phenomenon is strongly unsteady and that fluctuations on phase-averaged quantities are observed on a time scale in the order of a few milliseconds (at least during the systolic phase).

For a detailed knowledge of the flow field, velocity profiles are much more useful than vector maps; the former can be derived from the latter and compared for different times from the beginning of the heart cycle at a given position. In Fig. 6, several of these profiles along the transverse direction (x) for the axial velocity component (v) are reported; they are obtained at the widest measurement section which corresponds to the centre of the sinus of Valsalva (0.71 cm, i.e. about 0.4 D from the valve plane and $y/D=0.5$ in the image reference system). As previously noted, there is a strong variation (more than two order of magnitude) in the absolute value of the velocity during the cycle; the detection of such a high velocity dynamic range confirms the reliability of the PIV measurement technique for the present experimental conditions. Moreover, it is important to point out that during the systole the velocity profile shows an increasing asymmetry so that the flow coming from the left leaflet is faster than the flow from the right one (Fig. 6a). This phenomenon is observed even when two distinct jets coming from the leaflet openings are present (Fig. 6a); the configuration moves into a three jet condition during the systolic peak when at the centre of the field there is also an
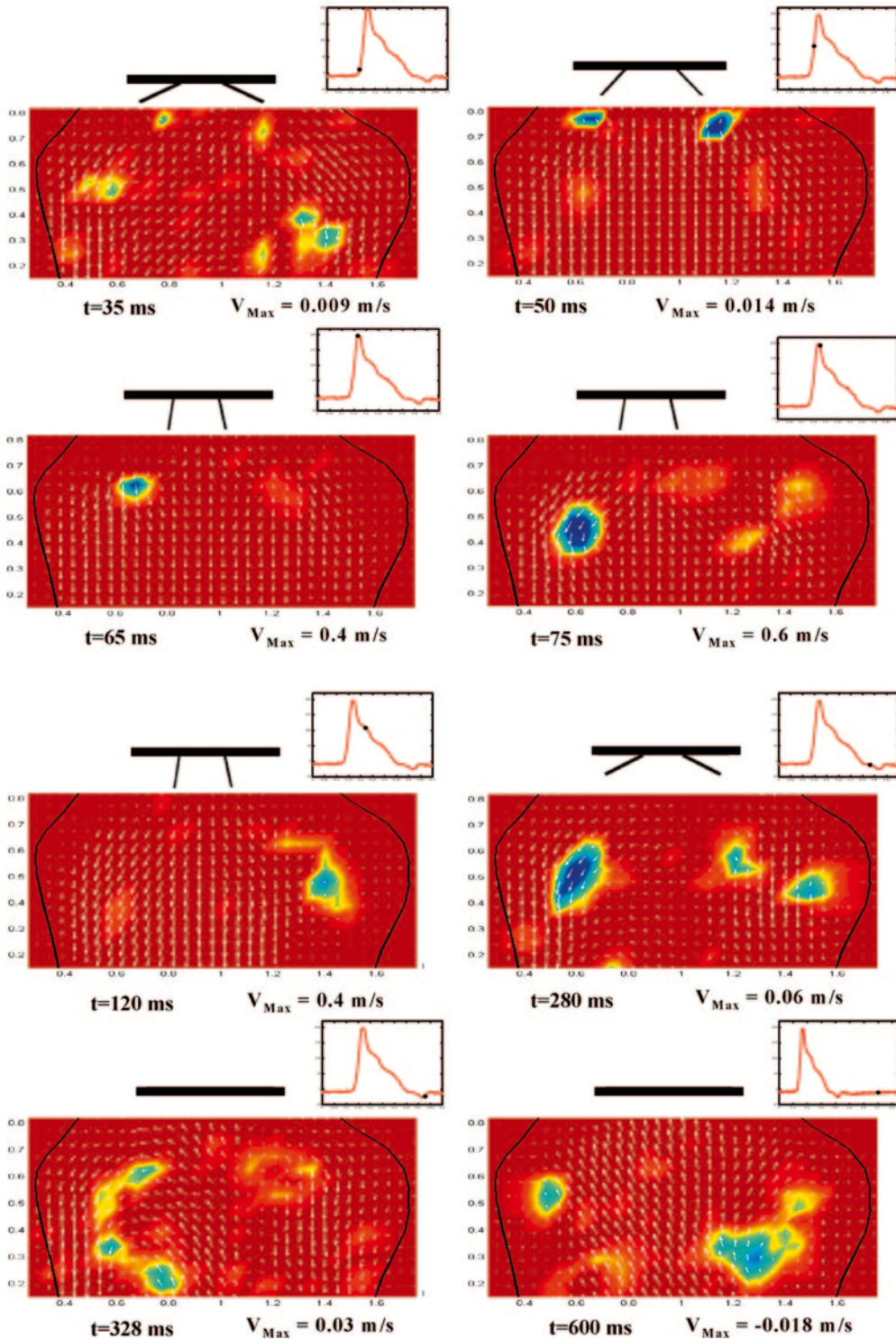
Fig. 5. Sequence of eight phase-averaged vector fields with overlapped vortex identification (Jeong and Hussain 1995). The position of the leaflets, the time interval from the beginning of the cycle, and the maximum positive or negative measured axial velocity are given for each field

effective flow (Fig. 6b). During the deceleration phase (Fig. 6c), the flow configuration returns to be almost symmetric showing a clear backflow also at the latest stage (even at this distance from the valve). The diastolic phase (Fig. 6d) is characterized by a constant velocity backflow, which is necessary to avoid fluid stagnation near the valve and the possibility of hinges failure. This backflow is confined to the central part of the test section, while on both sides there are recirculation regions which still give a forward flow (the rotation is opposite to what is observed during systole); even at $t \approx 600$ ms there is still a small forward flow region at the edges. The previous observations, coupled with those on the vortex in the sinus of Valsalva, suggest that the vortical structure in the sinus modifies the local flow field thus deviating the flow towards the left-hand side of the field. This should cause different forces on flow elements which pass on the left or right side of the valve.

One of the main features of an effective artificial heart valve is that it must not damage the blood cells, i.e. it
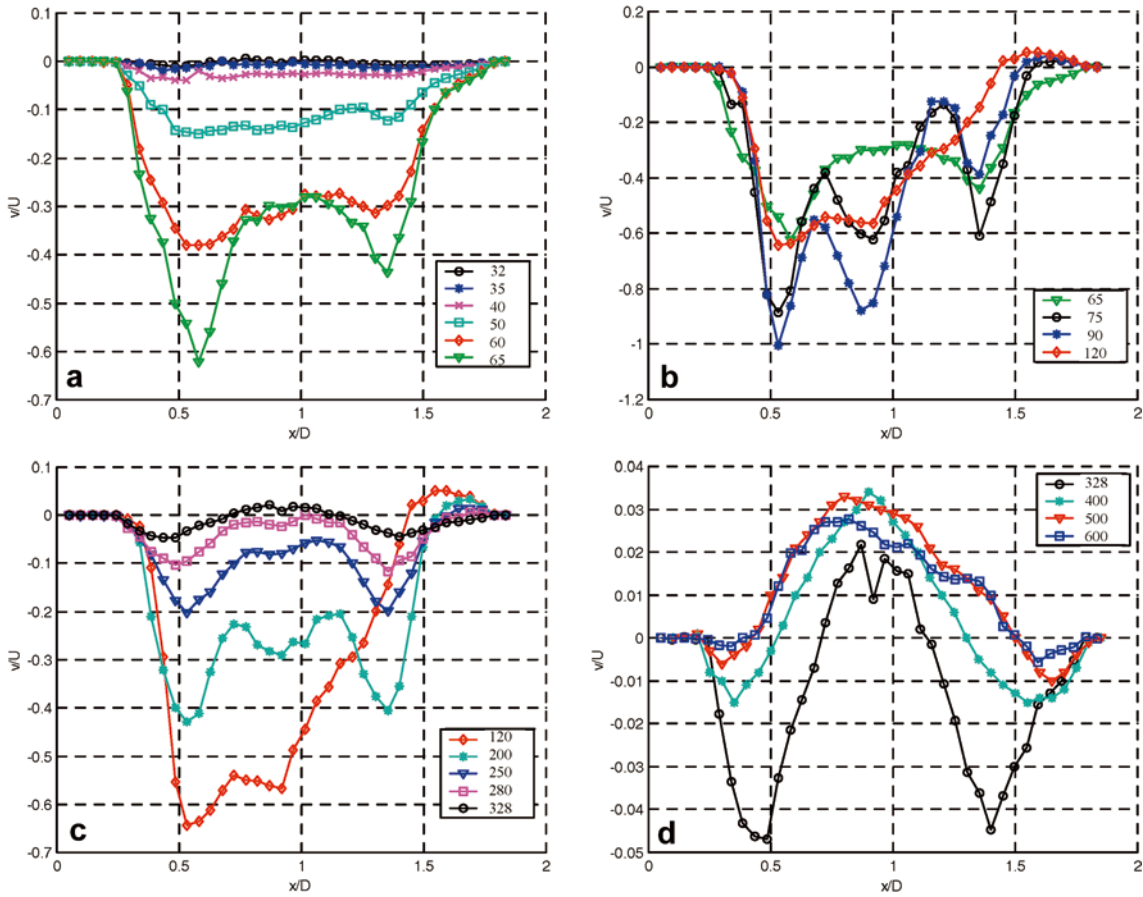
Fig. 6a–d. Sequence of phase-averaged axial velocity at a section corresponding to the centre of the sinus of Valsalva [y/D=0.5, corresponding to 0.71 cm (about 0.4 D) distance from the valve plane] obtained from PIV measurements. **a** t=32–65 ms, **b** t=65–120 ms, **c** t=120–328 ms, **d** t=328–600 ms
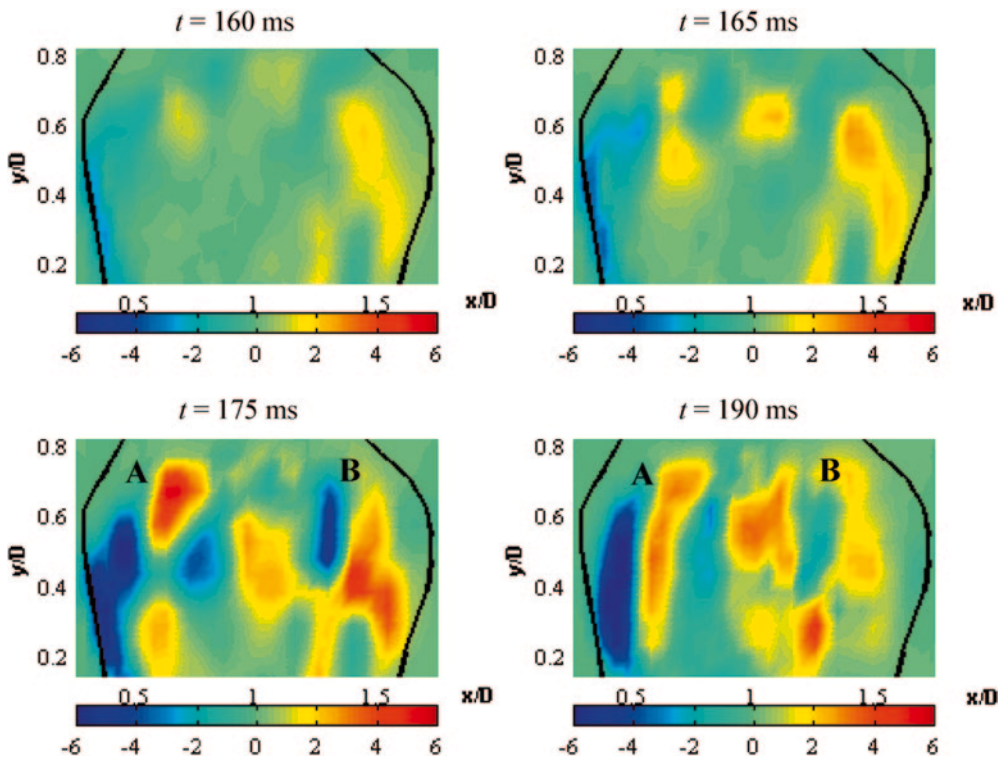

Fig. 7. Strain rate term e_{12} at four different phases non-dimensional by the characteristic size of the valve and by the peak velocity obtained from PIV measurements. The letters A and B indicate the two lateral shear regions

should not induce hemolysis; therefore, when investigating the flow field one should look at all the possible causes of cell damage. Large local deformations induced by the local velocity gradients may possibly be one the above-mentioned causes. They are measured by the strain rate tensor (i.e. the symmetric part of the velocity gradient tensor) and in particular by the off diagonal terms describing the shear. For the present field the term which can be measured is

$$e_{12} = \frac{1}{2}\left(\frac{\partial u}{\partial y} + \frac{\partial v}{\partial x}\right).$$

In Fig. 7, this quantity is shown at four phase-averaged instants which are selected in proximity of the systolic peak, when the highest values are measured. An elongated region of high deformation (close positive and negative values of e_{12}) grows in the shear layer which is generated between the left jet and the wall (labelled with A in Fig. 7); it reaches the maximum absolute value immediately after the systolic peak ($t=90$ ms). Simultaneously, a similar but less intense region grows in the right shear layer close to the sinus of Valsalva (labelled as B in Fig. 7). This produces the asymmetry already noticed in the phase-averaged mean velocity profiles.

Moreover, to take into account the effects of turbulence as well, the total stress (shear stress and Reynolds stress) is investigated:

$$\tau_{12} = \mu\left(\frac{\partial u}{\partial y} + \frac{\partial v}{\partial x}\right) - \rho\overline{u'v'}$$

whose profiles, measured at the same distance from the valve used in the velocity profiles, are given in Fig. 8. It is important to point out that the major contribution (more than 90%) to the total stress is given by the Reynolds stress so that the reported profiles are basically Reynolds stress profiles (the shear stress behaviour has been already given in Fig. 7). The four peaks observed during the systole correspond to the presence of the two jets (Fig. 8a); the Reynolds stress (especially on the left-hand part of the field) exceeds 5 N/m². The configuration changes after the systolic peak when the right and central part of the field attain the larger stresses (up to 50 N/m²). Therefore, the vortex structure in the sinus of Valsalva squeezes the jet passing through the right hole of the valve, toward the centre of the aortic root. This causes an increase of the velocity gradients at the interface between the fluid outgoing from the valve and the recirculating flow within the sinus of Valsalva. After the valve closes, the Reynolds stress decreases to values which are about 100 times smaller than before.

5
Results of PTV measurements

Preliminary PTV measurements have been also performed. In Fig. 9, the trajectories obtained by PTV before the systolic peak (Fig. 9a) and during the diastole (Fig. 9b) are given; the trajectories have a colour code which is related to the region where they cross the valve section (i.e. their starting location). It is clearly observed that particles from
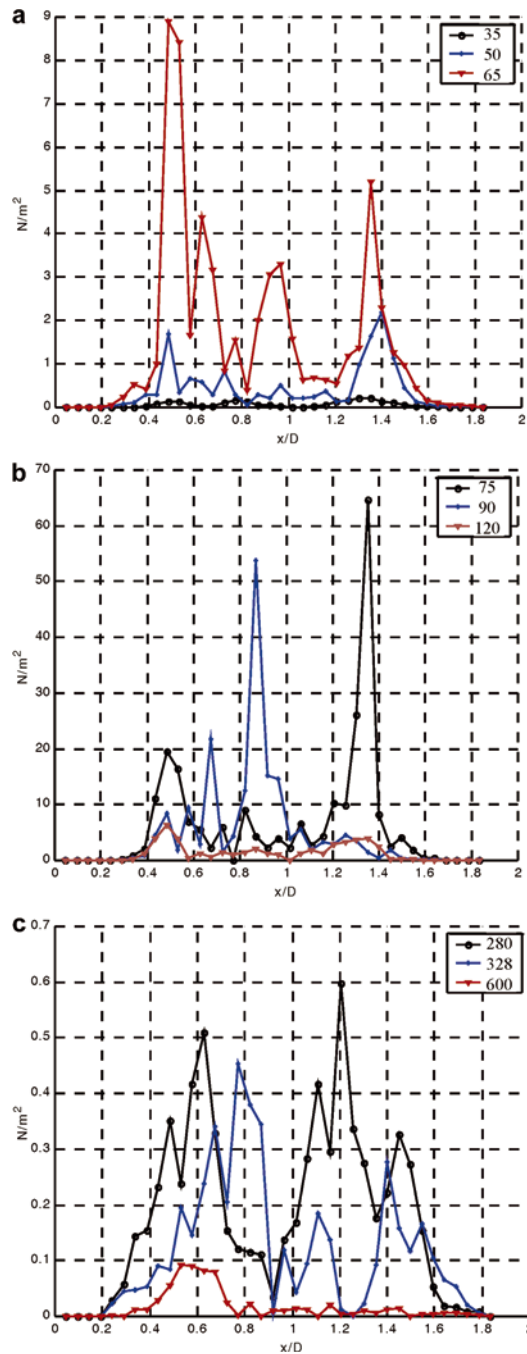
Fig. 8a–c. Sequence of phase-averaged total stress (shear stress+Reynolds stress) at a section corresponding to the centre of the sinus of Valsalva ($y/D=0.5$) obtained from PIV measurements. **a** $t=35$–65 ms, **b** $t=75$–120 ms, **c** $t=280$–600 ms

the region between the two leaflets (in blue) have almost no intersections with those from the side (in red) when considering a time interval before the systolic peak. On the other hand, the central jet spreads towards the boundaries during the diastole. During this phase, the recirculating motions within the sinus of Valsalva are completely established.

As described before, damage to the blood cells is related to the magnitude of the stress they suffer; nevertheless, the duration of the stress also contributes to the extent of the
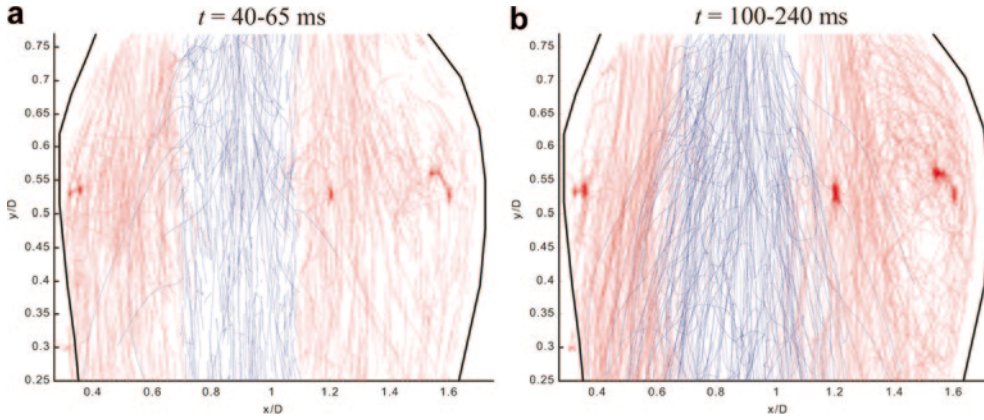
Fig. 9. Overlapping of particle trajectories measured by PTV during the time intervals $t=40$–65 ms (**a**) and $t=100$–240 ms (**b**) after the beginning of the heart cycle. *Blue* is used for trajectories crossing the valve section in the region between the two leaflets, while *red* is used for those passing externally

damage (Grigioni et al. 1999). As presented in Sect. 4, the magnitude of the stress (and/or deformation) can be obtained from Eulerian measurements. In addition, to measure how long the stresses are applied to a blood cell it is necessary to know the cell path-line and PTV is able to provide this kind of information (as shown in Fig. 9). Therefore, the detected PTV trajectories have been reconsidered in order to compute a reliable quantity which represents the mean time a particle spends in each region of the flow field. This information, combined with instantaneous maps of the total stress, is what is needed to describe the phenomena responsible for hemolysis. The mean residence time (MRT), T_R, is defined as the ratio of the total time spent by the particles in a given region to the number of trajectories crossing the same region:

$$T_{R,ij} = \frac{N_{H,ij} \times \Delta t}{N_{T,ij}}$$

where $N_{H,ij}$ is the number of times (i.e. successive time intervals) a particle was found in the sub-region ($x=i$, $y=j$), Δt is the time interval between frames, and $N_{T,ij}$ is the total number of particles in the same sub-region during the whole image acquisition time. Figure 10 shows maps of the MRT by subdividing the cardiac cycle into systole and diastole. It is apparent (and somewhat obvious given the low velocities) that globally the residence times are longer during the diastolic period than during the systole. Looking at the systole, the lower residence times are found in correspondence to the centre-left part of the aortic root, where higher axial velocities and almost straight path-lines are found. More interesting, the MRT increases towards the left wall (the one opposite to the sinus of Valsalva) since this is a zone where very high total stresses are measured (the sharp peak at the bottom-right part within the sinus of Valsalva is probably due to a reflection-generated image noise and has no physical meaning). The MRTs during the diastole, together with the plot of the total stress, indicate that this is not a critical phase of the cycle as the increase in the MRT is largely compensated by the decrease in the magnitude of the stresses.

6
Comments and conclusions
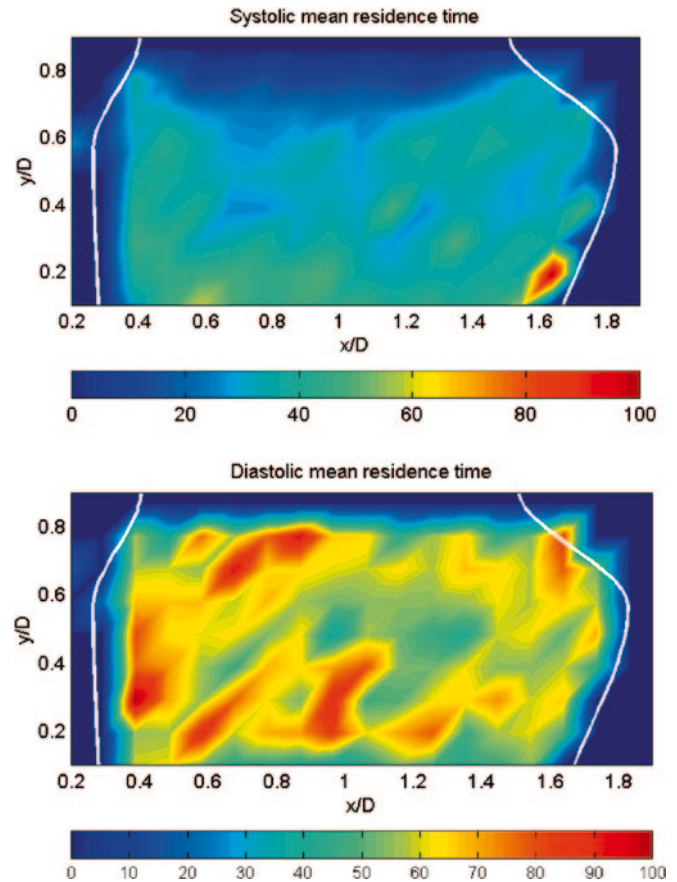Measurements of the velocity field downstream of an artificial heart valve are performed using both PIV and

Fig. 10. Mean residence time (in ms) for the systolic (*at the top*) and diastolic phase (*at the bottom*) of the cardiac cycle. Measurements by PTV

PTV techniques. The use of a high-speed video-camera allows the derivation of information both in time and space with quite a high resolution (the minimum measured displacement is about 0.1 mm and the time interval between data is about 1 ms) as required for investigations in the present inhomogeneous, anisotropic, and unsteady flow field. In particular, while the use of PIV enables one to obtain Eulerian statistics, for example, the magnitude of stress and strain components in given regions of the field, PTV is able to give fluid particle trajectories (i.e. Lagrangian statistics) and related quantities, for example,

the time interval a fluid particle spends in a given region of the field. Both these quantities must be used for a correct evaluation of the effective stresses on blood cells since the first one gives information about their magnitude, whereas the second one gives information about the duration they are applied to each blood cell.

The described PIV and PTV measurements allow us to underline the following characteristic features for the investigated flow field:

– The field is strongly inhomogeneous and unsteady; the assumption of homogeneous flow is not valid, while a steady flow can be assumed only in a time interval during the diastole.
– Large-scale vortices are detected especially in the sinus of Valsalva and in the wake of the valve leaflets; they are convected in time by the local velocity field without showing any major diffusion phenomenon.
– High strain rate and total shear stress on the measurement plane are measured, especially at the jet-wake interface downstream of the leaflets and close to the large-scale vortices; the magnitude of the strain and shear rate change more than two orders of magnitude from the systole to the diastole.
– The smaller mean residence time of fluid particles during the systole in comparison to the diastole partially compensates the effects of the higher stress and strain rate; a model which embodies both stress magnitude and duration (residence time) is required to asses and predict successfully the effective damage on blood cells for given fluid dynamic fields.

Of course, the complete knowledge of the three-dimensional field is required to describe possible damages on blood cells without errors; however, for a bi-leaflet valve (such as the one used in the present experiments) the plane orthogonal to the valve section is expected to display some of the most relevant aspects of the phenomenon. To evaluate the reliability of this assumption, measurements on different planes including the third velocity component are planned for the near future. Regarding this aspect, and in particular considering the Reynolds stress, it should be expected that in a full three-dimensional field the other components of this stress (in addition to $u'v'$) were of the same order of magnitude of those measured in the present work.

Finally, it should be noticed that any effect of the distensibilty of the aortic root has been neglected since a rigid model was used. Though these effects may be meaningful they imply many difficulties in the experimental investigation by means of optical methods such as PIV or PTV. Nevertheless, recent advances in research on structural materials suggest the possibility of building a model with distensible and transparent walls to perform such an investigation and to compare the results with numerical simulations.

References

Adrian RJ (1991) Particle image velocimetry for experimental fluid mechanics. Ann Rev Fluid Mech 23:261–304

Barbaro V, Grigioni M, Daniele C, D'Avenio G (1998) Principal stress analysis in LDA measurements of the flow field downstream of 19 mm Sorin Bicarbon heart valve. Technol Health Care 6:259–270

Bludszuweit C (1995) Model for a general blood damage prediction. Int J Artif Organs 9:583–589

Cenedese A, Querzoli G (2000) Particle tracking velocimetry: measuring in the Lagrangian reference frame. In: Particle image velocimetry and associated techniques, Lecture series 2000–2001, von Karman Institute for Fluid Dynamics, Belgium

Di Florio D, Di Felice F, Romano GP (2002) Windowing, re-shaping and re-orientation interrogation windows in particle image velocimetry for the investigation of flows with large velocity gradients. Meas Sci Technol 13(7):953–962

Fontaine AA, Ellis JT, Healy TM, Hopmeyer J, Yoganathan AP (1996) Identification of peak stresses in cardiac prostheses. A comparison of two-dimensional versus three-dimensional principal stress analyses. ASAIO J 42:154–163

Fung YC (1985) Biodynamics circulation. Springer, New York Berlin Heidelberg

Grigioni M, Daniele C, D'Avenio G, Barbaro V (1999) A discussion on the threshold limit for hemolysis related to Reynolds shear stress. J Biomech 32:1107–1112

Grigioni M, Daniele C, D'Avenio G, Barbaro V (2000) On the mono-dimensional approach to the estimation of the highest Reynolds shear stress in a turbolent flow. J Biomech 33:701–708

Grigioni M, Daniele C, Morbiducci U, Di Benedetto G, D'Avenio G, Barbaro V (2001) Towards hemolitic potential evaluation by using CFD (Part I: venous canulation study). In: IFMBE proceedings Medicon

Jeong J, Hussain AKMF (1995) On the identification of a vortex. J Fluid Mech 285:64–94

Kini V, Bachmann C, Fontaine A, Deutsch S, Tarbell JM (2001) Integrating particle image velocimetry and laser Doppler velocimetry measurement of the regurgitant flow field past mechanical heart valves. Int J Artif Organs 25:136–145

Krafzyk M, Cerrolaza M, Schulz M, Rank E (1998) Analysis of 3D blood flow passing though an artificial aortic valve by Lattice–Boltzmann method. J Biomech 31:453–462

Ku DN (1997) Blood flow in arteries. Ann Rev Fluid Mech 29:399–434

Lim WL, Chew YT, Chew TC, Low HT (1998) Steady flow dynamic of the prosthetic aortic heart valves: a comparative evaluation with PIV techiniques. J Biomech 31:411–421

Lu PC, Lai HC, Liu JS (2001) A re-evaluation on the threshold limit for hemolysis in a turbulent shear flow. J Biomech 34:1361–1364

Reul H, Van Son J, Steinseifer U, Schmitz B, Schmidt A, Schmitz C, Rau G (1993) In vitro comparison of bileaflet aortic heart valve prothesis, St Jude Medical, CarboMedics, modified Edward–Duromedics and Sorin Bicarbon valves. J Thora Cardiovasc Surg 106:412–420

Steinman DA (2000) Simulated pathline visualization of computed periodic blood flow patterns. J Biomech 33:623–628

Zimmer R, Steegers A, Paul R, Affeld K, Reul H (2000) Velocities, shear stresses and blood damage potential of the leakage jets of the Medtronic Parallel bileaflets valve. Int J Artif Organs 23:41–48